Study of the thermomechanical behavior of UHMWPE yarns under different loading paths

Coline Roiron, Eric Lainé, Jean-Claude Grandidier, Dominique Olivier, Nicolas Garois, Cathie Vix

Study of the thermomechanical behavior of UHMWPE yarns under different loading paths

Coline Roiron[1,4*], Eric Lainé[1], Jean-Claude Grandidier[1], Dominique Olivier[2], Nicolas Garois[3] and Cathie Vix[4]

[1]*Institut Pprime, UPR3346 CNRS, ISAE-ENSMA, Université de Poitiers, F-86962 Futuroscope Chasseneuil Cedex, France*

[2]*Total Research & Technology Feluy, Zone Industrielle Feluy C, B-7181 Seneffe, Belgium*

[3]*Centre de recherche Hutchinson, Rue Gustave Nourry BP31 F-45120 Châlette-sur-Loing, France*

[4]*TOTAL S.A., Tour Coupole La Défense, 2 Place Jean Millier, F-92078 Paris, France*

*Corresponding author:
Coline Roiron
coline.roiron@ensma.fr

ABSTRACT: UHMWPE viscoelastic fibers show great interest as reinforcement within composites and especially when used in SRPs (Self-Reinforced Polymers). They provide ductility, lightness and recyclability, benefits that glass or carbon fibers cannot provide. It is, therefore, necessary to increase knowledge about the behavior of UHMWPE fibers. Before the thermomechanical characterization of these yarns, an experimental protocol is proposed, validated and it supplements the existing standard. Monotonous, load-unload and creep tensile tests were carried out on Doyentrontex® yarns. Temperature and strain rate dependencies were observed. A time-temperature superposition is used to reconstruct the evolutions of modulus at 0.5%, maximum strength, and strain at break at 23°C over a wide range of strain rates. The behavior of the yarns studied appears to be complex. Indeed, at low temperatures, a hyperelastic type of behavior, combined with plasticity, predominates whereas a more elasto-viscoplastic one emerges at 100°C. From creep tests, a time-temperature-stress level superposition leads to the reconstruction of the yarns creep behavior over a long period at the reference temperature 23°C and the reference stress level, which is 40% of the stress at break in tensile tests at any given test temperature.

Keywords: yarn test protocol; commercial yarn behavior; viscoelasticity; hyperelasticity; creep and tensile tests

1 INTRODUCTION

Glass fiber reinforcements are present in 95% of the composites produced in 2018 [1]. However, the glass and carbon fibers reinforcements raise questions about the regulations on waste management and the ever more stringent environmental legislation, in the automotive industry for example, in addition to the industrial requirements related to the lightness of the structures. Glass, carbon and natural fibers can only be recycled into new reinforcing grades but whose mechanical properties are degraded. A first answer to these issues could be the use of thermoplastics. Indeed, thermoplastic matrices are already widely used today. Thus, a new concept of Self-Reinforced Polymers (later called SRP) was then proposed by Capiati and Porter [2]. It is a composite material constituted by a single polymer, whose matrix and reinforcement are of the same chemical family. SRPs combine lightness, ductility, good cost/performance ratio, and recyclability. Thus, these materials make it possible to fill the gap, in terms of mechanical and thermal properties, between unreinforced and glass-fiber reinforced polymers while being recyclable and lightweight [3-10]. For example, compared to conventional composites, SRPs stand out above all for their high energy absorption capacity and therefore their impact resistance [6,7,11-12]. This latter ability makes this material a very good candidate for military uses, for instance [13-15].

The ductile nature of SRP is given by viscoelastic fibers, which therefore seem to be of great interest. But polymers have mechanical properties that do not correspond to the theoretical maximum, because their molecular structure is very weakly oriented. The alignment of molecules by different processes (by solid-state extrusion or drawing from a gel solution) is a means of producing fibers with high mechanical performance, in particular very high modulus and strength. The structure of the fibers has been studied in detail [16-18]. Their morphology depends on the initial material (chain length, degree of entanglement and crystalline morphology) as well as on the processing technique and, particularly on the type of extrusion. Thus, the properties of the composites are highly dependent on their mechanical processing.

Many authors have focused on studying unique fibers [19-26] also called filaments by some. It is tedious to extract a single fiber from the package and to perform numerous tests on very small diameter fibers. Besides, it is very complex to accurately measure the cross-section of a single fiber [26]. Thus, the data reported in the literature or by manufacturers are averaged data given the experimental difficulties associated with measuring cross-sections. Entering precise values for mechanical parameters is complex because they depend on chemical and process aspects [8]. For all these reasons and because SRP are made of yarns, the study will focus on yarns and not fibers. Besides, understanding yarn behavior is a necessary step in predicting the response of tissues within a matrix of the same nature. Most studies focused on Dyneema® (DSM) [14, 19-21, 27] or Spectra® fibers (Spectra) [23].

In this framework, many authors have already studied the effect of temperature on UHMWPE fibers [20-21, 28]. The effect of strain rate has also been the subject of several studies. At low speed, a distinct yield strength was observed and subsequently disappeared [23]. At higher speeds, there is a trend in the literature towards more elastic behavior. Indeed, Russell et al. [14] observe this by evaluating the behavior of yarns over a wide range of strain rates and these results are confirmed [23]. However, Kromm et al. [20] deny any dependence on the mechanical properties, modulus and strength, to the strain rate for tests between 1%/min and 100%/min, except for elongation at break. The authors attribute this to the high degree of crystallinity of the fibers in a given direction following the drawing process, which results in the reduction of the viscoelastic contribution.

Similar influences of time and temperature appear. An increase in strain rate and/or a decrease in temperature leads to an increase in fiber modulus and fiber strength as well as a decrease in work at fiber failure [27, 29-30]. Furthermore, a brittle/ductile transition is highlighted due to the temperature, which is associated with a change in morphology among others [28]. Indeed, in the same way as with temperature, a transition appears with the strain rate [30]. In the ductile region, the strength increases with the enhancement of the crossbar speed. In the brittle region, no influence of the strain rate is perceived. Govaert and Peijs [29] outlined that at low temperatures and/or high strain rates, the fibers show a brittle behavior and a high dependence on strain rate and temperature for tensile strength. At high temperature and/or low strain rate, a transition from brittle to ductile fracture can be observed.

To fully characterize UHMWPE fibers, creep properties were examined too, which are also highly dependent on temperature and time. A decreasing exponential reflects the temperature dependence of the strain rate [20,29]. In the same way as Dessain et al.[21], Kromm et al. [20] find, in the case of creep tests, changes in behavior that depend on the imposed stress and the temperature. An apparent critical stress that does not allow permanent creep is speculated by Wilding and Ward [31]. Some authors have been involved in modeling creep behavior [22, 29, 31–33]. A time-temperature superposition was also identified [34]. As the impact of temperature and strain rate has been analyzed, curves can also be superimposed in tension. From two curves obtained at two different temperatures and strain rates, a time-temperature superposition appears possible [24]. Similarly, such a superposition is performed from tensile tests to reconstruct the strength and modulus at 1 % using two different Arrhenius law. The associated activation energy is 115 kJ/mol for modulus and 85 kJ/mol for strength [27, 29]. A master curve of the stress relaxation modulus in the linear viscoelastic region is also obtained from tensile tests carried out at several temperatures and true strains [34]. In DMA, according to an Arrhenius law, a master curve is reconstructed by superimposing the measured dynamic modulus [26, 32, 34-35]. In addition to monotonous and creep tensile tests, the behavior of UHMWPE fibers was analyzed in cyclic tension with recovery [30]. However, to the author's knowledge, no load-unload tests at different temperatures have been performed to date to identify the mechanical behavior.

Most of the work dates to before the 2000s. With the attractiveness of the introduction of SRPs in the composite industry, it is necessary to increase knowledge on the properties of UHMWPE fibers, and to focus on the compaction effect of fibers and the load-unload behavior at different temperatures.

Following a bibliographical search, to the author's knowledge, these last points, as detailed upstream, constitute breaches of the literature. To overcome this and understand the complex thermomechanical behavior of UHMWPE fibers between hyperelasticity, viscoelasticity, and viscoplasticity and to be able to describe the transition between ductility and brittleness, an experimental campaign is carried out. It includes tensile tests under monotonous load, at several strain rates and temperatures, but also increasing load-unload tests at different temperatures and, finally, temperature creep tests at several loading levels. Above all, a test protocol needs to be developed and validated. Because in some cases the standard may seem insufficient to ensure the validity and the reproducibility of the tests. The yarn setup, the cross-section to consider and the useful length must be determined with care.

In the first section, the material studied is presented as well as the different equipment used. Then, in a second section, the test protocol is detailed. The choices made are justified to validate the experimental protocol and they will be used for each test. In a third section, the behavior of

commercial yarns in tension at different temperatures and strain rates is described and analyzed, as well as the behavior in load-unload and creep.

2 EXPERIMENTAL

2.1 Material

The fibers used for the tests were extracted from a spool of Doyentrontex® yarns, gel-spun PE. One yarn is made of many fibers. As indicated by the manufacturer, the modulus is over 1210 g/d, considering that 1 g/d = 0.883 cN /dtex and 1 cN /dtex = 95.098 MPa and the elongation at break is less than 4%. This type of commercial fibers is poorly or not characterized in the literature, to the author's knowledge.

2.2 Testing method

Tensile and creep tests were conducted on an INSTRON 1195 screw machine, controlled in terms of crossbar speed. A resistance furnace, manufactured in the lab, was slid around the specimen for test at raised temperatures. Tensile tests were carried out until complete rupture, at room temperature, 40, 60, 80 and 100°C. Creep tests were performed by requiring the machine to hold the load on the fiber steady at the chosen load at room temperature, 60°C, 100°C, and at 40%, 60% and 80% of the breaking load at each temperature. The choice of the useful length and the loading speed will be explained in detail below.

The yarn tests were performed according to the C 1557-03 standard [37]. A yarn was therefore glued with a Loctite® glue on a piece of paper to facilitate its positioning on the test machine (Figures 1). The heels of this paper frame are folded back to prevent damage to the yarn when the jaws are tightened. The lateral edges of the frame are then cut so that only the yarn is loaded. The standard applies to all types of fibers, in strands or spools. The test speed must be sufficient for the yarn breakage in less than 30 seconds. And any twisting of the yarn must be avoided as this reduces the value of the tensile strength. The cross-section to be considered must also be measured close to the breaking point, but if the fiber bursts, the energy released during the break must be braked by grease, for example.

The section considered for stress calculation is the section measured under an optical microscope upstream and averaged over several samples. The nominal diameter of the yarn thus taken into account is 500 µm. Regarding the elongation, and since the use of extensometers on such small samples is complex to implement, elongation is calculated from the displacement of the crossbar. In this way, the measurement made corresponds to the elongation of the sample but also that of the machine. However, the greatest contribution of this displacement is between the jaws. Since the loads used do not exceed 10% of the device limit, the displacement related to the machine can be neglected.

Figure 1. (a) Picture of a tested sample; (b) Picture taken through the window of the furnace, of a sample set up on the test machine

3 PROPOSITION AND VALIDATION OF AN EXPERIMENTAL PROTOCOL

3.1 Development of the experimental protocol

According to the standard, tests were then carried out in monotonous and increasing load-unload. In monotonous loading in Figure 2a, all the yarns tested alike do not seem to be stressed from the beginning and multiple breaks are visible, meaning a heterogeneous alignment of the fibers constituting the yarn which can lead to the invalidation of the test [38]. Some peaks are associated with late fiber loading. To ensure that all fibers have been stressed and that the load has been distributed evenly, the test is considered valid if the fibers are completely separated. The presence of wave in the yarn may be a cause of this non-uniform load [27]. The failure seems to happen in the useful length, so there is no stress concentration close to the jaws. Regarding the curves obtained in load-unload tension in Figure 2b, the tests carried out in the same conditions, appear to be difficult to reproduce. Yarns are very sensitive to handling, preparation, and packaging [17-38]. Surface defects have a major influence on the mechanical properties and diversity of the curves drawn. Differences in stiffness can also be explained by the uncertainties regarding the diameter of the yarns [20]. This parameter will be deeply studied below.

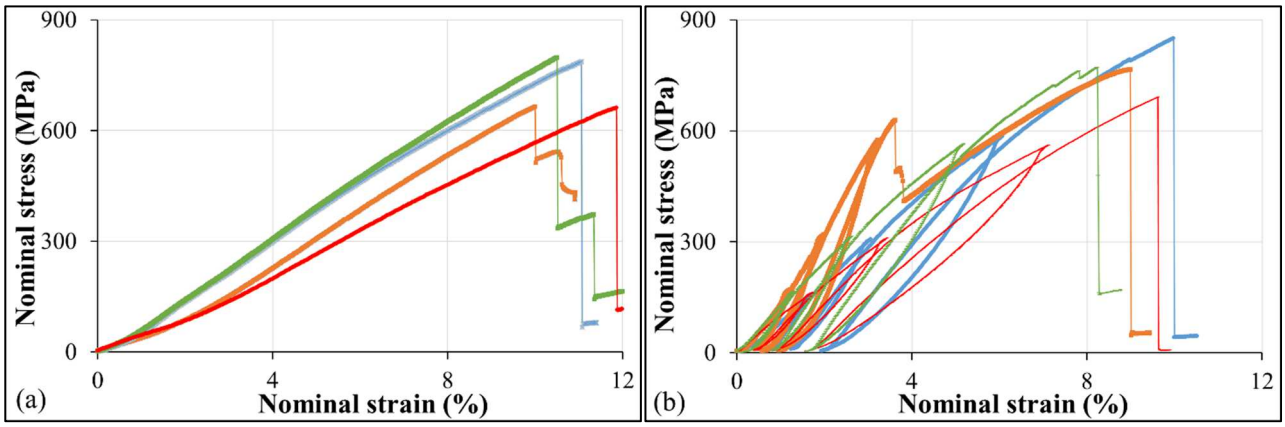

Figure 2. Nominal stress/nominal strain curves in tensile – (a) monotonous tension - (b) load-unload

Several ways of twisting the yarn have been tested to determine the influence of the way the yarn was set up. A pre-tension of a few Newton's is also applied at the beginning of the test. These different ways are listed in **Table 1**. MEOX defines the different setup way with X the increment.

Table 1: Details of the different tested ways to set up the yarn

Name	Number of twists	
	at one end	at the other end
MEO1	4	4
MEO2	1	1
MEO3	2	3
MEO4	0	0

When 4 twists are imposed at each end of the yarn for the MEO1 (Figure 3a), the twisting angle is very important. The load is no longer only in tension but also in shear. Friction occurs in this case as well. Damage can then be created [38], leading to early rupture. In the case of a twist on each side in Figure 3b, the mechanical response is variable. A small twist results in staggered reorientations of the constituent fibers. Figure 3c shows, for the MEO3 setup, only the most extreme responses. The tests are therefore highly reproducible compared to the other setups. No early damage is visible, and the realignment of the fibers is identical in both cases presented. This setup thus seems to stabilize the geometry. Finally, for the MEO4 setup, previously described in Figure 2a, no twist is applied. Yarns are not loaded from the beginning of the test and the stress distribution is not uniform since the failure is multiple.

So, the protocol is somewhat modified and deviates from the standard. The tests are thus more reproducible, the yarns are stressed from the beginning of the test and the failure is unique, proof that all the fibers are identically stressed. This second protocol, using the MEO3 setup, will be followed for all the other tests conducted.

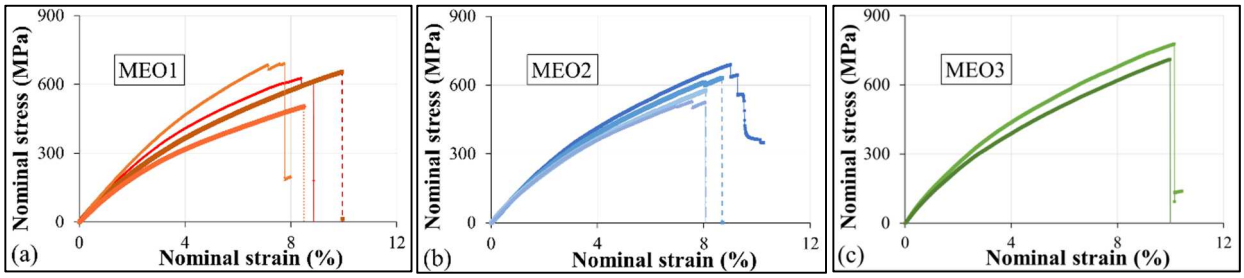

Figure 3. Nominal stress/nominal strain curves in tensile loading for: (a) MEO1, (b) MEO2, (c) MEO3

Standard C 1557-03 [37] stipulates that the failure must occur within 30 seconds of the start of the test. However, a test whose speed is sufficient to cause the yarn to break in less than 30 seconds will cause it to burst. The failure zone cannot then be located. To slow down the energy released during rupture, the tested yarns are coated with silicone grease. Figure 4 illustrates the nominal stress/nominal strain curves, which are greatly different with or without the addition of grease. The strain at break and the maximum stress reached are much lower when using grease. This suggests that the presence of grease limits the compacting effect by filling voids. So, no grease will be added in the rest of this study. The crossbar speed is reduced to be able to visualize the location of the failure and be certain that the failure is not occurring near the jaws. It will be 0.9 mm/min for further testing.

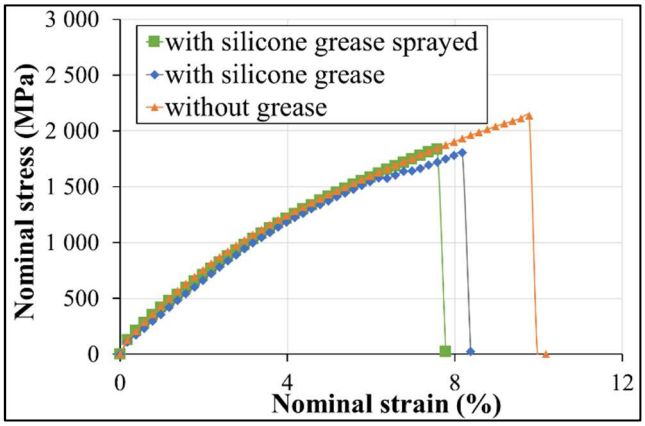

Figure 4. Nominal stress/nominal strain curves of tensile tests on commercial UHMWPE yarns with or without silicone grease

3.2 Cross-section to consider

While for most tests, the strain is calculated with the displacement of the crossbar. Two different methods are applied to determine the true longitudinal strain: a marker tracking software, IdPix, which is developed at the ISAE-ENSMA and the post-processing of the recorded pictures during the test by the CCD camera, with the free software Fiji.

A video camera records some pictures of the two markers made on the tested yarn. IdPix is then able to identify the border of the marker and calculate its barycenter and track its movement. Using a finite difference method, it measures the true strains during the test. The second technique consists of measuring variations in the section and length of the markers on the recorded pictures. The choice of marker type is important. Pen ink infiltrates into the fibers. Consequently, a mask was then created and associated with black spray paint, which sharpens the borders of the marker and reduces the variation in the position of the barycenter. Figure 5a compares these two methods which allow the determination of the true longitudinal strain. This strain obtained with the software IdPix retains jumps and shows its limits at the end of the test, just before the failure. The one obtained by Fiji envelops it during the first three-quarters of the test. The transverse strain was only calculated by exploiting the pictures. The strains achieved are very high: up to -20%, as remarkable in Figure 5b. This seems to corroborate the yarn compaction during the test and the presence of voids between fibers, compaction previously observed during the tests with the addition of grease.

The section actually used does not, therefore, seem to be the one previously considered (500 µm diameter). Optical or laser measurements cannot consider the section actually tested. To avoid the presence of voids, several samples were embedded in epoxy resin as Russell et al. did [14]. The different embedded yarns are cut in the center using a diamond disc and each of the ends is studied. Polishing is complex because the two materials are very different, and a certain topology exists on the surface. Their sections could then be observed using an optical microscope (Figure 6a). The fibers that make up the yarn have been counted. On average, 406 fibers constitute a yarn and they are continuous in the samples examined. Their cross-sections were averaged over sixty measurements and the diameter is about 14.02 µm (Figure 6b). These fibers are not perfectly circular, and this is due to the drawing process. This process induces a variation in the cross-section [20]. The cross-section to be considered in the following tests takes into account this average diameter as well as the number of fibers in a yarn. This change in section results in an increase in maximum strength achieved from 750 MPa to 2400 MPa on average.

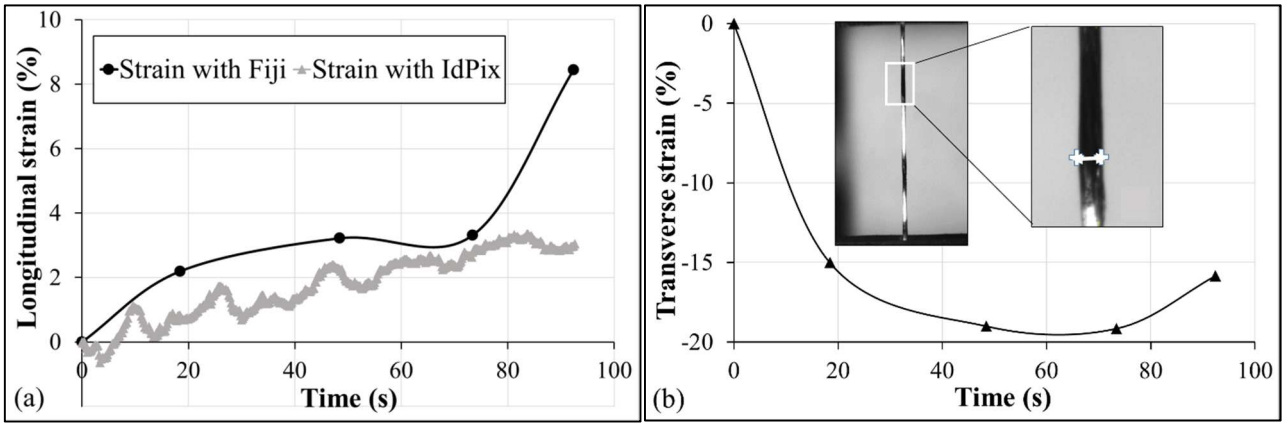

Figure 5. (a) Comparison of true longitudinal strains obtained with the two methods used; (b) Transverse strain during the test, determined from image processing

To overcome the imperfect circularity, many authors calculate the section from the density [14, 17, 20, 23-24, 38-39]. Even when studying a single filament, the section varying from one point to another during tensile tests, R'Mili and Murat [38] ensures that in the literature, under no circumstances, the true section is known.

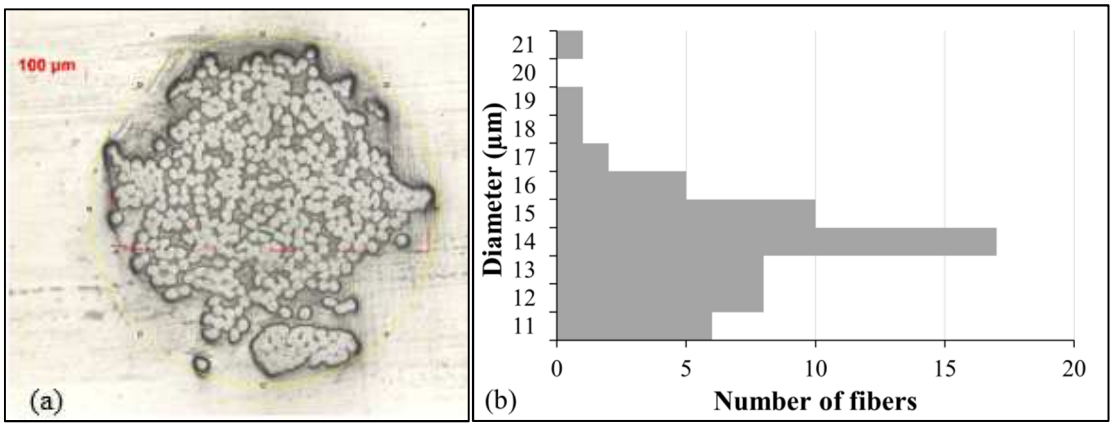

Figure 6. (a) Observation under an optical microscope of a cross-section of a yarn embedded in a resin; (b) Diagram describing the variability of the cross-section of the fibers constituting the yarn

3.3 Determination of the appropriate useful length

The influence of the useful length (l_0) was also studied. The optimal length is the one that is large enough to be representative of the spool while being less than the frequency of defects. Indeed, for Dyneema® filaments [20], the longer the useful length, the higher the friction forces and therefore the more successful the selection of filaments. This invalidates tests done on long useful lengths because of the selection effect and on short lengths because the volume is not representative of the diameter fluctuation. But, the frequency and type of defects depend on the grade of the fiber studied and the process used. The different grades of fibers examined by Wilding and Ward [22] (BP Chemical, Rigidex 50) no longer show variations in properties above 6 cm of useful length. However, for the type of UHSPE fibers considered by Schwartz et al. [23] and for tests between 10 and 200 mm, no influence of the useful length is observed. Long fibers are as strong as short ones. For them, the only thing that can justify this is either a distribution of critical defects over a small period (less than 10 mm in this case) or a single type of defect that appears at high frequency.

Three useful lengths (l_0) were tested: 12, 15 and 20 mm at 0.9 mm/min. 3 tests were performed at each length and they are reproducible. Figure 7a shows a single curve for each length. As defined previously, the optimal length is the one that is large enough to be representative of the spool while being less than the frequency of defects. The influence of the useful length is marked. The mechanical properties are much reduced for a length equal to 20 mm. The frequency of defects in the fibers is, therefore, less than 20 mm. The maximum moduli and strengths are close for 12, and 15 mm samples. Thus, 15 mm seems to be the optimal length since it is less than the frequency of defects while maintaining good mechanical properties. For that reason, the useful length considered for the rest of the tests conducted will be 15 mm.

3.4 Influence of yarn relaxation

The influence of yarn relaxation on the mechanical properties was evaluated. Tensile tests were carried out on yarns directly extracted from the spool and yarns which were extracted 48 hours before the test. Yarns testing were performed at 0.9 mm/min, in tension. Three tests were done for both cases and plotted in Figure 7b. Relaxed yarns have on average a strain at break and modulus equivalent to those of directly extracted yarns. The maximum strength is on average slightly lower for yarns extracted 48 hours before. However, given the complexity and sensitivity of the yarns tests, no influence of yarn relaxation on mechanical characteristics can be concluded.

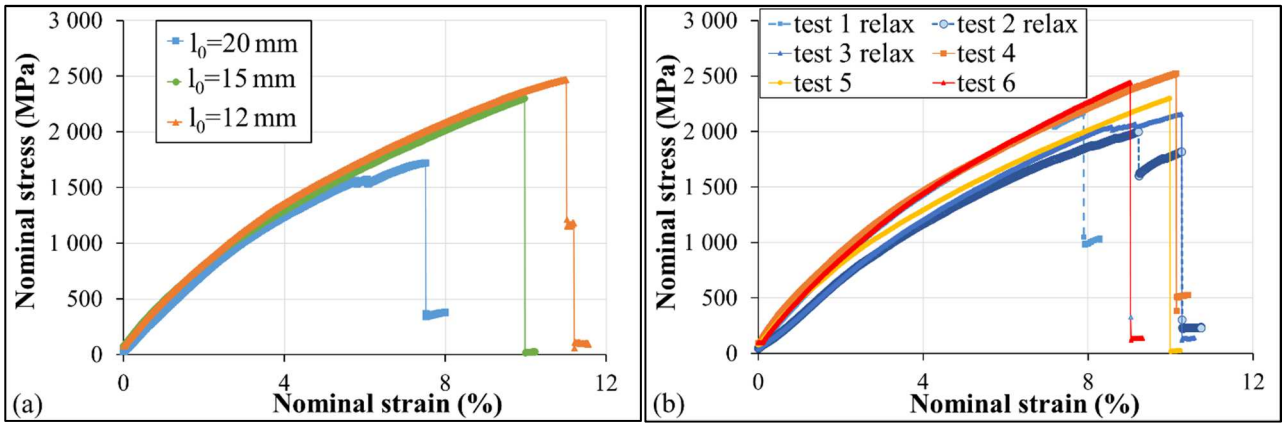

Figure 7. Nominal stress/nominal strain curves of tensile tests: (a) for several useful lengths - (b) on relaxed and unrelaxed yarns on commercial UHMWPE yarns

3.5 Discussion

These first studies made it possible to establish a test protocol for the following tests. Thus, standard C 1557-03 [37] appears insufficient to carry out the tests and must be reconsidered. Indeed, the deviation of C 1557-03 from the way the yarns are set up is justified by the greater reproducibility of the tests, the uniform loading of all the fibers as well as the almost immediate loading of the fibers. Moreover, the reduction of the test speed to 0.9 mm/min relies upon the possibility of locating the breaking point to ensure that the jaws do not damage the yarns. Afterward, the yarns will be tested according to the MEO3 setup, at a crossbar speed of 0.9 mm/min. The section considered is calculated from the number of fibers (406 on average in a yarn) multiplied by the assumed circular average section of fiber. This enables to be free from the compaction effect identified. Thereafter, the yarns will be tested under the conditions described above: according to the MEO3 setup, at a crossbar speed of 0.9 mm/min which is locally equivalent to 10^{-3} s^{-1} and a useful length of 15 mm.

4 RESULTS AND DISCUSSIONS

4.1 Traction

4.1.1 Influence of the temperature

For monotonous tensile tests, five temperatures have been considered: 23, 40, 60, 80 and 100°C, at 0.9 mm/min. For the same temperature, at least three samples were tested to verify the reproducibility of the tests. As the curves are reproducible, a single curve is plotted for each test temperature in Figures 8. A significant influence of temperature is noticeable on the strain at break, the maximum stress reached, the modulus as well as the failure mode. Indeed, stiffness and maximum strength decrease with temperature while strain at break increases at higher temperatures. Thus, at 23 and 40°C, the behavior appears to be brittle with low strain at break while at higher temperatures, the behavior is more ductile with higher strains at break. A brittle/ductile transition seems to occur between 40 and 60°C. At higher temperatures, the shape of the response is quite like that of a non-drawn semi-crystalline polymer.

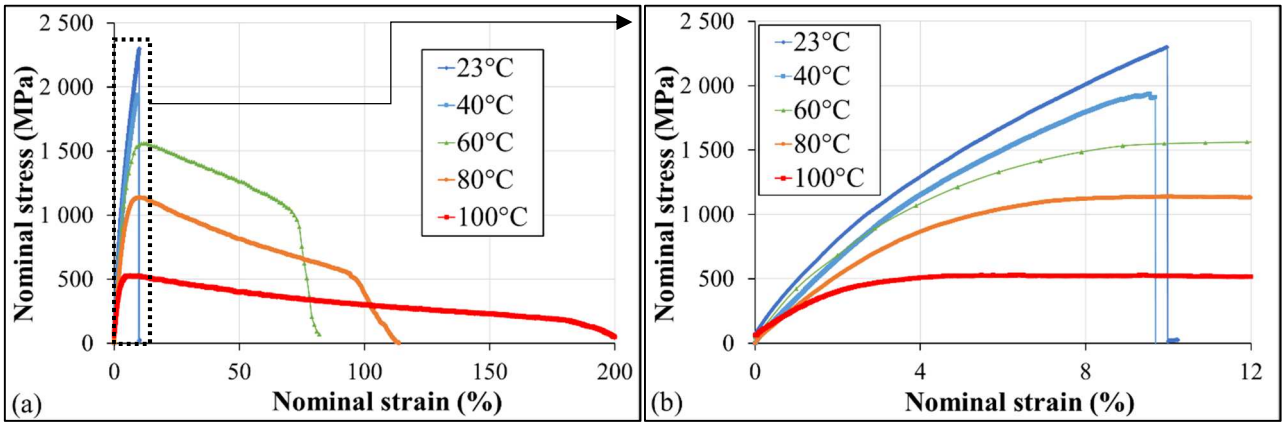

Figure 8. (a) Nominal stress/nominal strain curves of tensile tests on UHMWPE commercial yarns at several temperatures; (b) Zoom of nominal stress/nominal strain curves of tensile tests on UHMWPE commercial yarns at several temperatures

The focus is on the variation of the different parameters: modulus, maximum strength, and strain at break with temperature. Figures 9 plot the average of these parameters which is calculated on at least 3 tests. Error bars indicate the extreme values obtained experimentally. The same trends are

visible for each of the parameters. Indeed, at 23 and 40°C, the values of the parameters are rather stable and for 60, 80 and 100°C, there is a significant drop in the modulus at 0.5%, noticeable in Figure 9a, and the maximum strength in Figure 9b. Over this temperature range, the influence of temperature seems linear and stronger. The slope change occurs between 40 and 60°C, in line with the brittle/ductile transition previously observed. The transition value, given the three parameters studied is within the temperature range of [42°C-47°C]. On Dyneema® fibers, Dessain et al. [21] point out a modification in the slope of a fiber's strength at 5°C and Dijkstra et al. [24] at 20°C for non-commercial fibers. This is related to a change in morphology. This transition temperature between brittle and ductile behavior is dependent on the type of fibers as it is greatly impacted by the process conditions. This point would need clarification in another paper.

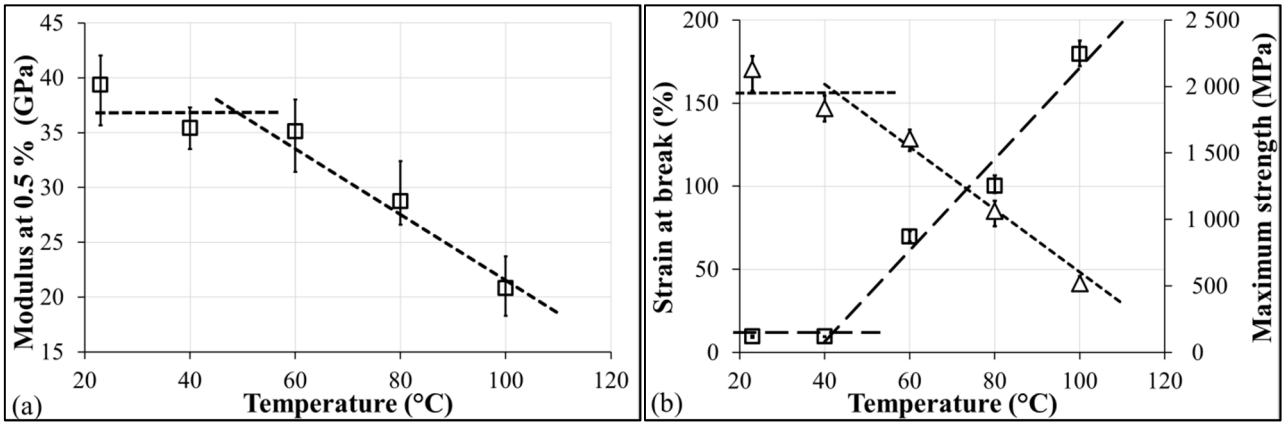

Figure 9. Influence of the temperature on: (a) modulus at 0.5% - (b) maximum strength and strain at break

4.1.2 Influence of the strain rate

In addition to being tested at a crossbar speed of 0.9 mm/min, tensile tests on yarns were also performed at 0.09 mm/min and 9 mm/min at the same temperatures to evaluate the influence of the strain rate on their behavior. This corresponds locally to speeds of 10^{-2}, 10^{-3} and 10^{-4} s^{-1}. For one temperature and one strain rate, at least three samples were tested to verify the reproducibility of the tests. The modulus at 0.5%, the maximum stress reached and the strain at break are measured and plotted on average as a function of the local strain rate in a logarithmic scale in Figures 10. Error bars indicate the extreme values obtained experimentally.

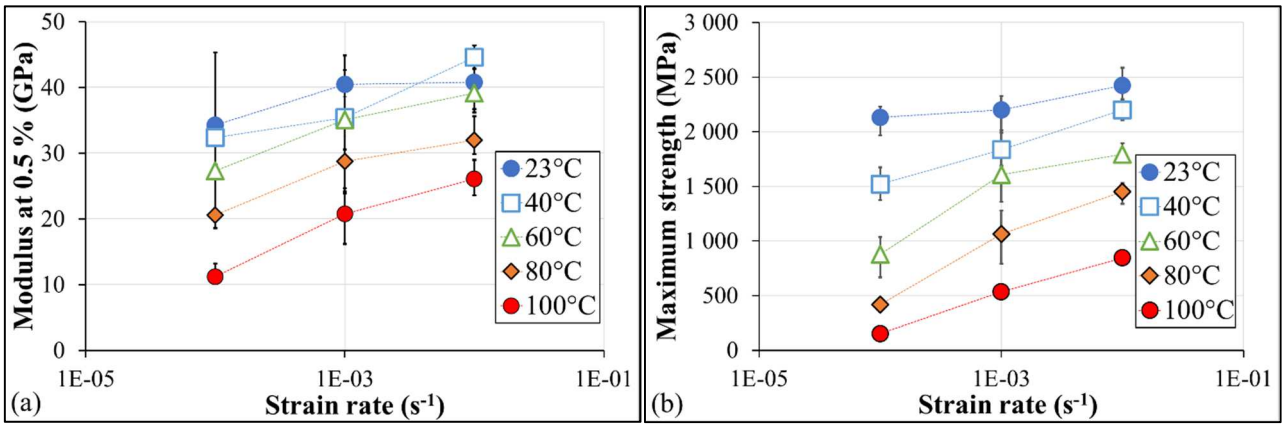

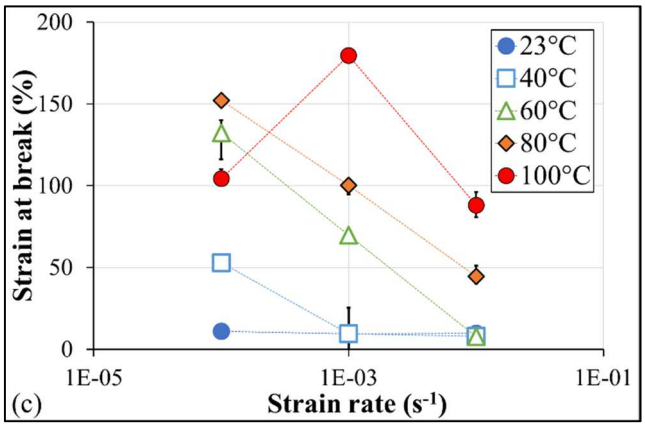

Figure 10. Variation of (a) the modulus at 0.5%, (b) maximum strength, and (c) strain at break of the commercial yarns studied, as a function of the local strain rate, in a logarithmic scale

For each temperature, the maximum strength and modulus at 0.5% of the yarns increase with the strain rate, while the strain at break decreases at higher local strain rates. Moduli at a given strain rate increase with temperature, except at a strain rate of 10^{-2} s^{-1} at 23 and 40°C. This can be explained by the variability of the yarns and the sensitivity of the experimental tests on the other hand. Indeed, the error bars overlap partially at 23°C and 40°C at 10^{-2} s^{-1}. Similar influences of time and temperature are well established and conformed to the literature on other commercial types of UHMWPE yarns [27, 29-30]. The difference between the values of these parameters at several temperatures decreases with strain rate. However, one point deviates from these trends. This is the failure strain of the tests conducted at 100°C and 10^{-4} s^{-1}. Indeed, the strain at the rupture point is just beyond 100% whereas it is well above 180%, at a strain rate of 10^{-3} s^{-1}. This may be related to a different morphology at such a temperature and, therefore, to chain conformations that does not allow greater deformations for this strain rate. This deflection, to the writer's knowledge, is not mentioned in the literature.

4.1.3 Time-Temperature Superposition Principle (TTSP)

In this part, time-temperature equivalence is evaluated on UHMWPE yarns. The reference temperature chosen is 23°C. The various parameters studied (modulus at 0.5%, maximal strength, and strain at break), and therefore the associated nominal stress/nominal strain curves, are horizontally translated to obtain a master curve. Several laws are proposed in the literature to define shift parameters such as, for example, in this study:

$$\sigma_{max}(\dot{\varepsilon}, T_1) = \sigma_{max}(a_T * \dot{\varepsilon}, T_2) \quad (1)$$

The WLF equation is usually used to define the shift factor for amorphous polymers above the glass transition $[T_g; T_g + 100°C]$. In some cases, the WLF equation is not valid for semi-crystalline polymers at temperatures below their melting point. Seitz and Balazs [40] have suggested that in this case, the description of the shift factor follows an Arrhenius equation. Thus, in this study, two different shift laws are used to determine the shift factor a_T, which is therefore identical for each parameter as the maximum strength reached, the 0.5% modulus and the strain at break. A WLF law (eq 2) or a modified Arrhenius one (eq 3) [40] could be thus applied:

$$\log(a_T) = \frac{-C1*(T-T_0)}{C2+T-T_0} \quad (2)$$

$$\log(a_T) = \frac{\Delta H}{2.303*R}\left(\frac{1}{T} - \frac{1}{T_0}\right) \quad (3)$$

With $C1$and $C2$, two variables depending on the material and the reference temperature, T the temperature and T_0, the reference temperature (23°C), ΔH the activation energy and R the universal gas constant. The two appropriated parameters $C1$ and $C2$ of this law are 41 and 712 K respectively (Figure 11a). For most common polymers, their characteristic values are 15 and 50 K. The difference in our case can be explained by the drawing process which modifies the PE originally used. Concerning the proposed Arrhenius law, an activation energy of 107 kJ/mol is obtained to be able to represent the shift factors. Concerning the superposition of the modulus of UHMWPE Dyneema® yarns, an activation energy of 115 kJ/mol for modulus is determined in the literature [27, 29]. The result obtained in this study is quite consistent given the differences related to the process and the initial structure of the material. The shift factors are in good agreement with the factors experimentally got. Figure 11a shows that those obtained from WLF seem slightly more satisfactory as noticeable.

The time-temperature superposition principle applied to the maximum resistance and the modulus at 0.5% leads to a linear increase in these parameters as a function of the local strain rate, in logarithmic scale, and then to a stabilization of these parameters (Figure 11b and c). As regards the strain at break (Figure 11d), it decreases linearly with the strain rate up to 10^{-4} s^{-1} and then becomes independent of the rate beyond 10^{-4} s^{-1}. Thus, the behavior appears to be independent of the strain rate above approximately 10^{-4} s^{-1}. The threshold is around 10^{-4} s^{-1} and is slightly shifted for the maximum strength. Following tensile tests over a very wide range of strain rates on Dyneema® yarns, Russell et al. [14] show this transition phenomenon for all parameters at the same strain rate, 10^{-1} s^{-1}. Schwartz et al. [23] observe a transition between viscoelastic behavior and elasticity at a strain rate of about 1.7 10^{-3} s^{-1} on Spectra® fibers. Therefore, such a transition appears to be generic. Besides, as described above, one point does not follow the trend, that at 100°C and 10^{-4} s^{-1}. Another transition appears to occur at very low strain rates for Doyentrontex® fibers. The main transition is strongly related to the object of the study (fiber or yarn), the morphology, and therefore to the process conditions, and consequently to the type of fibers.

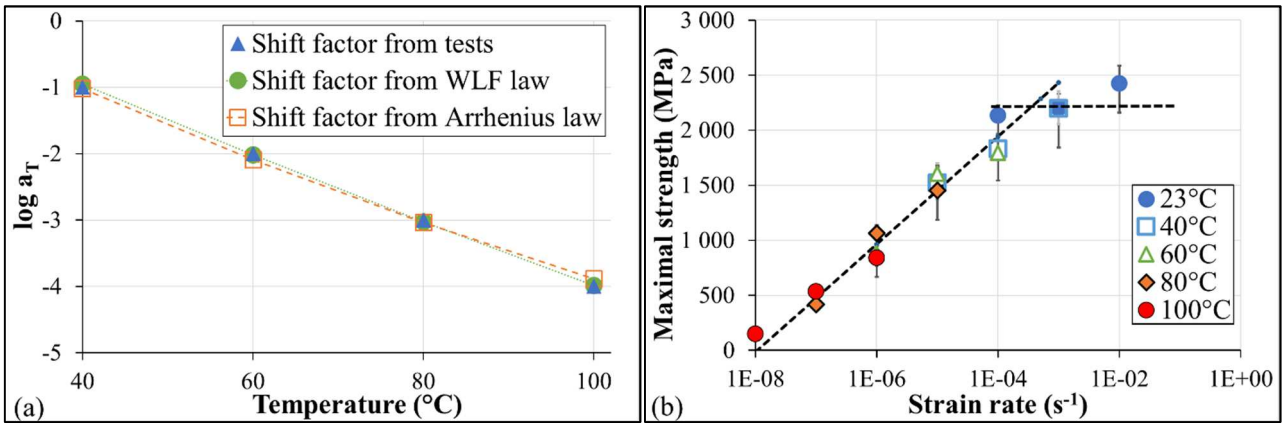

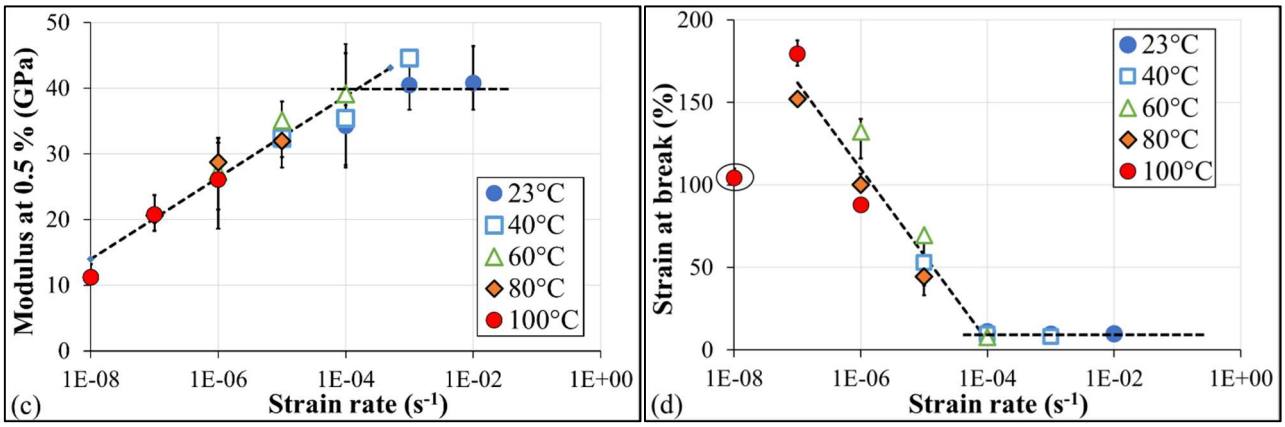

Figure 11. (a) Comparison of the shift factors that allowed the horizontal shift of the following parameters; Time-temperature superposition, at a reference temperature of 23°C (b) of the maximum strength, (c) modulus at 0.5% and, (d) strain at break, obtained from tests carried out at several temperatures and several strain rates on commercial yarn

4.2 Load-unload: hysteresis

To characterize the mechanical behavior, increasing load-unload tests have been performed. This behavior must be considered at several temperatures regarding the intended applications for SRPs. Thus, non-recoverable load-unload tests were performed at 23, 60 and 100°C and 10^{-3} s^{-1} and plotted in Figures 12. For each temperature, two tests were conducted, and they appeared reproducible. As a result, a single curve will be presented each time as well as a tensile curve at the same temperature. At the two lowest temperatures, the cycles were made around 1.6%, 3.2%, and 6.3% of nominal strain. At 100°C, the cycles correspond to 0.8%, 2% and 4.7% of nominal strain, because at this temperature, 6% of nominal strain coincides with a stress that is above the yield point.

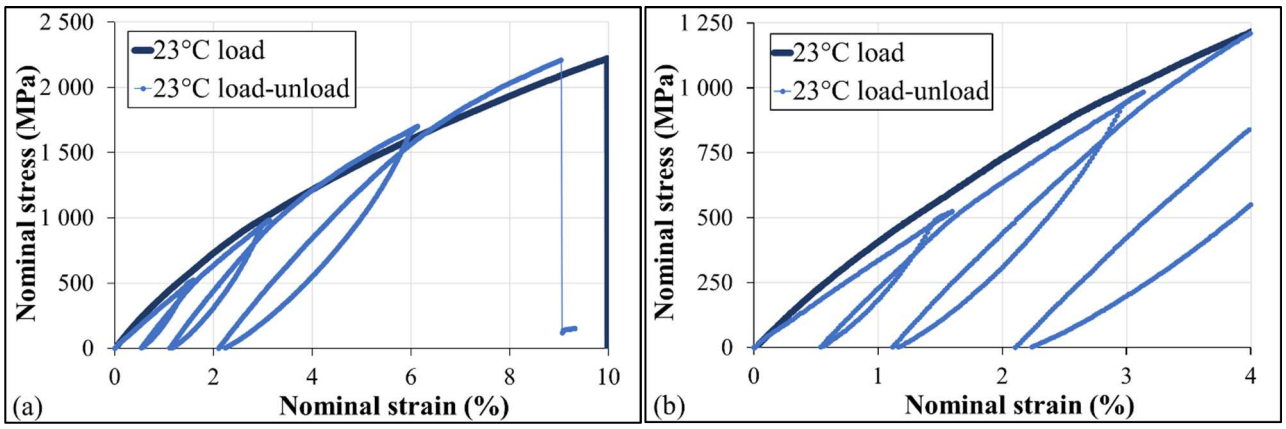

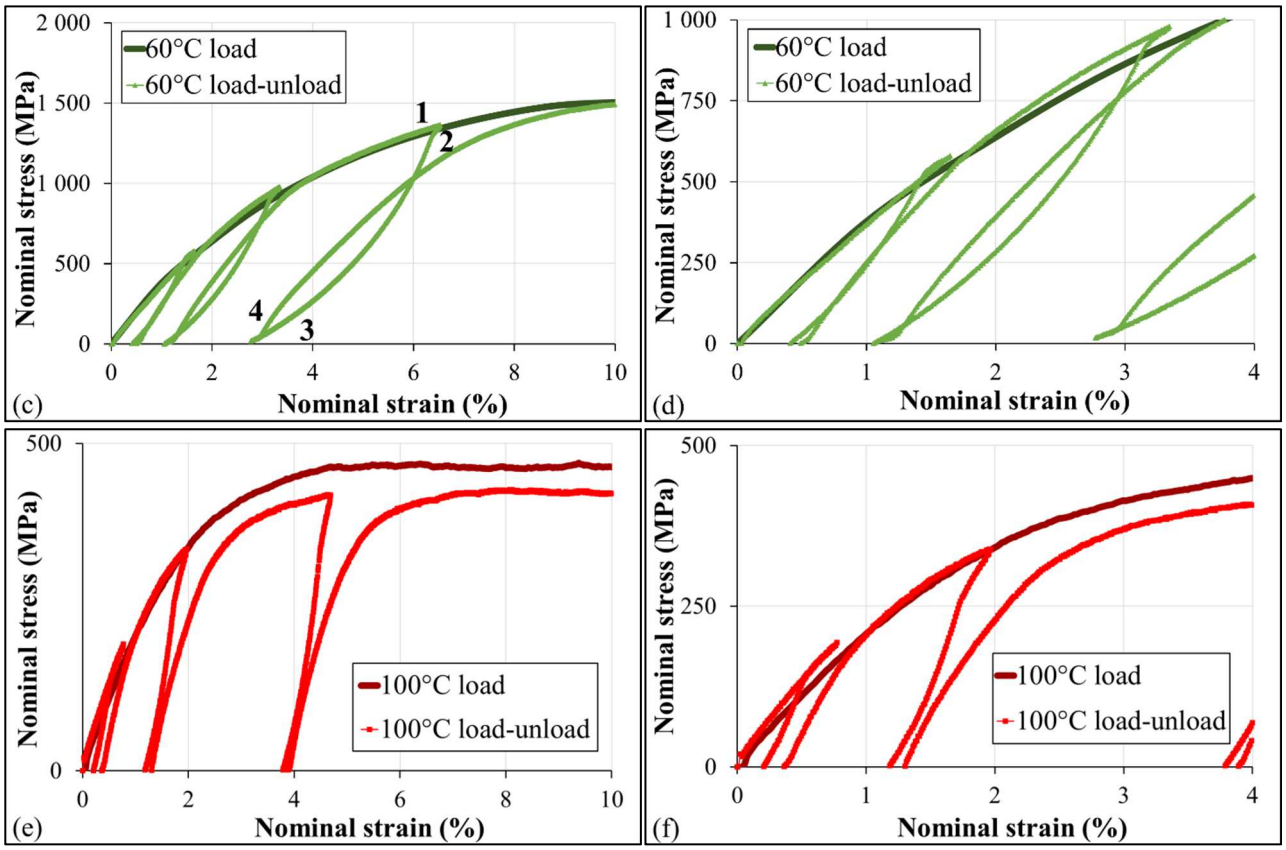

Figure 12. Nominal stress/nominal strain curves of tensile tests and load-unload tests on UHMWPE commercial yarns at (a) 23°C, (c) 60°C and (e) 100°C; Zoom of nominal stress/nominal strain curves of tensile tests and load-unload tests on UHMWPE commercial yarns at (b) 23°C, (d) 60°C and (f) 100°C

Hysteresis is the expression of viscosity. At 23 and 60°C, the first loop is almost closed, proof that this is still the elastic range. No energy is associated with viscous phenomena. At 23°C, a slight counter-curvature is visible when unloading begins. At 60°C, counter-curvatures are much more observable at the beginning of unload and reload and at the end of the cycle. These counter-curves suggest a "hyperelastic" type of behavior at these temperatures. This type of behavior is comparable to the Mullins effect that appears for elastomers. At 100°C, counter-curvatures are somewhat less observable at the beginning of unload and reload and the end of the cycle. But the introduction of a twist when the yarn is set up in the proposed experimental protocol is another hypothesis that could explain these counter-curves. When unloading, the imposed twist slightly delays the return of the yarn to a less deformed state. Fibrils extension may be a twist effect. Figures 13 show that load-unload tests were then carried out with yarns set up in other ways (MEO1 and MEO2 **Table 1**) at 23°C. In both cases, and therefore, whatever the number of twists imposed, the counter-curvatures are present. This indicates that these are the effect of the behavior and not the way the yarns are tested. More importantly, at 100°C, the hysteresis does not form a loop. As a result, the viscosity is very low. The type of behavior is more like elasto-viscoplasticity. The studied yarn tends towards flow. The effect of viscosity is still found in the shift in the curve between the beginning of unloading and reloading. It would be necessary to relate these findings to the physical state of the yarns.

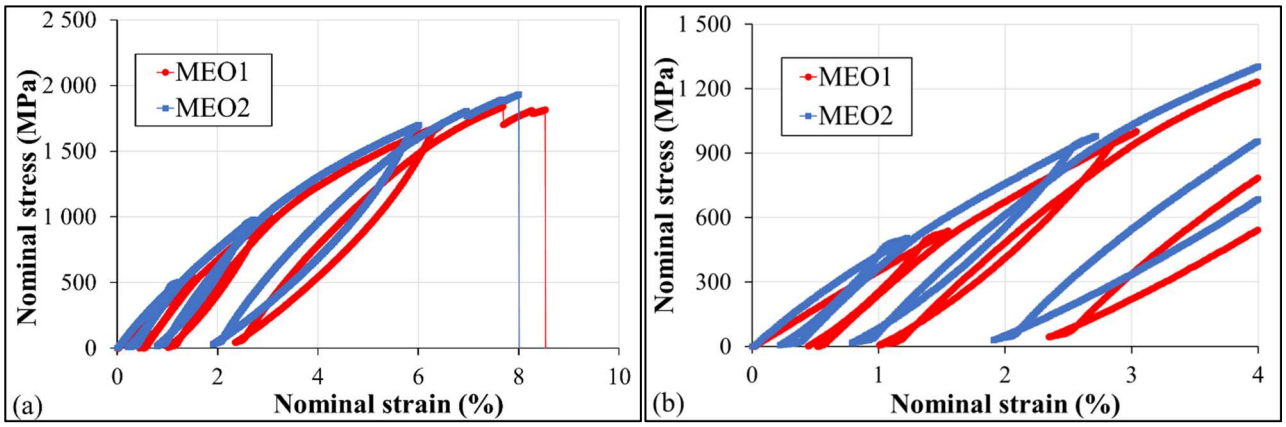

Figure 13. (a) Nominal stress/nominal strain curves of load-unload tests on UHMWPE commercial yarns at 23°C set up with the MEO1 and MEO2 ways; (b) Zoom of nominal stress/nominal strain curves of load-unload tests on UHMWPE commercial yarns at 23°C set up with the MEO1 and MEO2 ways

The loops, therefore, have a very different shape depending on the test temperatures. The tangent moduli E_T were measured and values were reported in **Table 2** at several key points of the curves: at each end of loading and unloading, locations 1 and 3 indicated on the Figure 12c, and at each beginning of unloading and reloading, locations 2 and 4 reported on the same figure for the three cycles at 23, 60 and 100°C.

Table 2: Tangent moduli measured at different locations on the hysteresis loops at 23°C (a), 60°C (b) and 100°C (c)

(a)	Nominal strain	Test temperature	E_T (GPa) Location 1	Location 2	Location 3	Location 4
Loop 1	1.6%	23°C	32.3	71.8	38.2	49.7
Loop 2	3.2%	23°C	30.4	73.7	32.2	46.7
Loop 3	6.3%	23°C	21	70.3	26	46.9
(b)	Nominal strain	Test temperature	E_T (GPa) Location 1	Location 2	Location 3	Location 4
Loop 1	1.6%	60°C	31.7	66.4	39.7	54.7
Loop 2	3.2%	60°C	20.5	66.9	26.8	50.4
Loop 3	6.3%	60°C	12	65.3	18.7	49.5
(c)	Nominal strain	Test temperature	E_T (GPa) Location 1	Location 2	Location 3	Location 4
Loop 1	0.8%	100°C	21.8	51.9	35.7	39.6
Loop 2	2%	100°C	10.6	32.7	33.1	39.6
Loop 3	4.7%	100°C	2.1	42.7	34.3	38.1

At 23 and 60°C, the tangent moduli are similar at the beginning of the unload (location 2), which is not the case at 100°C, and at the beginning of the reload (location 4), regardless of the loop considered. At this highest temperature, the tangent moduli at the end of the unload (location 3) and at the beginning of the reload (location 4) are very closely, whatever the loop. Sliding of the base of the hysteresis occurs, the mechanical history seems to be erased. Again, a change in behavior is observed between 100°C and lower temperatures. A different chain conformation of the yarns studied at different temperatures seems to be confirmed and phase transformation should be the cause.

4.3 Creep tests

Creep tests were finally carried out to fully characterize the behavior of the commercial yarns studied. These tests were performed at three different temperatures, at 23, 60 and 100°C, and at several loading levels, at 40, 60 and 80% of the maximum load causing the failure in each case. For the load increase, the crossbar moves at 0.9 mm/min. At least two tests were conducted for each condition. In creep, the tests are less reproducible than tensile or load-unload tests because, in the third phase of creep, the influence of the variability of the yarns and their defects is predominant [21]. The values given will be averages and a representative curve will be presented for each situation examined in Figures 14.

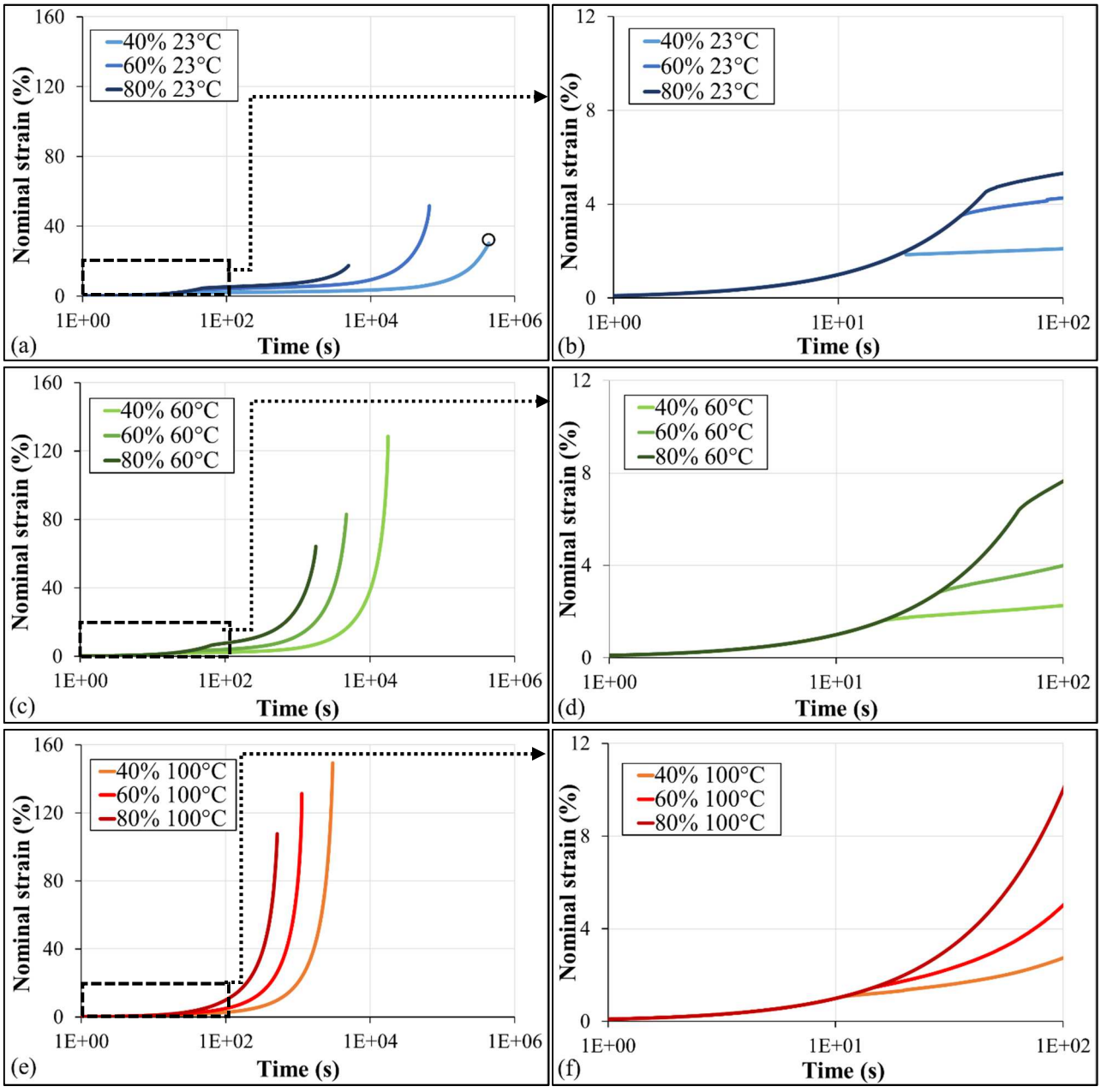

Figure 14. Nominal strain vs time curves of creep tests at different load levels at (a) 23°C, (c) 60°C and (e) 100°C; Zoom of the primary creep mode on the nominal strain/time curves of creep tests on UHMWPE commercial yarns at different load levels at (b) 23°C, (d) 60°C and (f) 100°C

The creep test performed at 23°C at 40% of the maximum load for more than 5 days did not fail as noticeable in Figure 14a. The classic polymer flow system is found, characteristic of their

viscous flow. Figure 14a, c, and e show that creep kinetics present the three conventional zones: primary, secondary and tertiary creep. The size of these zones depends on the temperature. The secondary zone, for which the slope is almost horizontal, decreases with the temperature and it is practically absent at 100°C. At this highest temperature, the tertiary zone is nearly only observable. At this last temperature, the phases present, and the associated chain conformations must facilitate the sliding of the chains to each other.

Creep kinetics accelerate with temperature. Indeed, the average fracture time and strain at break are plotted as a function of the load level applied in creep for each test temperature in Figures 15. Error bars indicate the extreme values obtained experimentally. A power law and a linear law make it possible to predict the averaged time to break and the averaged strain at break, respectively, at these three temperatures for any loading level. At 23°C, for the lowest load level, the test was not long enough to cause failure. The unfilled points are extrapolated from the suggested laws described in Figures 15.

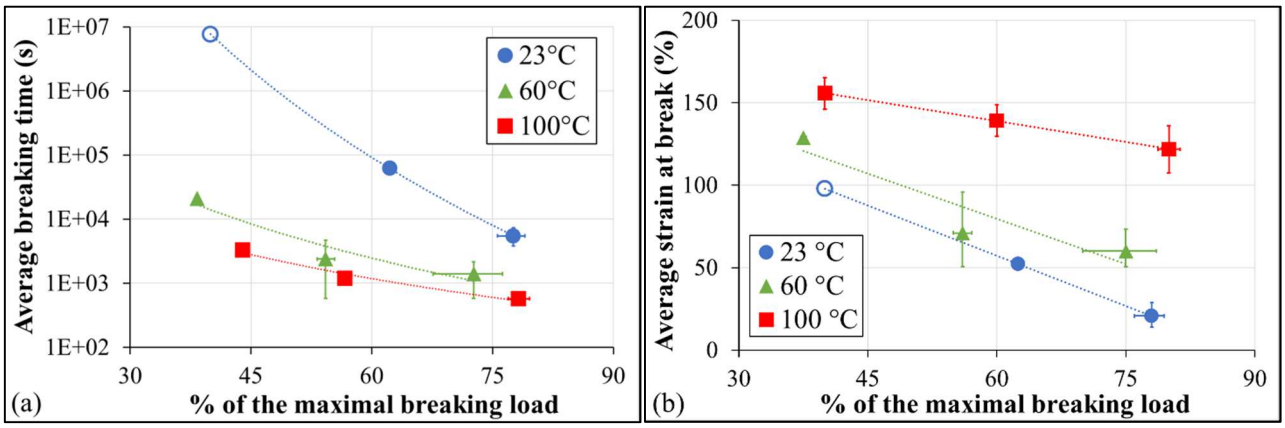

Figure 15. Curves showing (a) the average breaking time and (b) the average strain at break as a function of the percentage of the maximum breaking load, as a result of creep tests

For the same level of load, i.e. 40%, 60% or even 80% of the maximum load leading to failure for each test temperature, the creep compliance vs time curves obtained at different temperatures seem to be able to overlap by shifting them horizontally (Figure 16a, b, and c). Creep compliance is defined as the ratio of creep strain to the reference stress level at the given temperature. For example:

$$\mathrm{D}(23°\mathrm{C}, 40\%, \mathrm{t}) = \frac{\varepsilon(t)}{0.4 * \sigma_{break}(23°C)} \quad (4)$$

$$\mathrm{D}(100°\mathrm{C}, 80\%, \mathrm{t}) = \frac{\varepsilon(t)}{0.8 * \sigma_{break}(100°C)} \quad (5)$$

Master curves can then be defined. The curves shifting is given by an Arrhenius law for semi-crystalline polymers [40]. The reference temperature chosen is 23°C. Figure 16d plots the linear temperature dependence of the shift factors a_T experimentally obtained. The higher the load level, the lower the temperature dependency. This first time-temperature superposition leads to sub-master curves. A time-stress level superposition is carried out in a second step. From the sub-master curves presented in Figure 16a, b, and c, a horizontal shift is made and a final master curve is gathered in Figure 16e. Luo et al. [41] proposed a time-temperature-stress superposition (TTSSP) on PMMA. For this, a WLF type of law is adapted to determine the shift factors of the time-temperature superposition and the time-stress superposition. In the study carried out on Doyentrontex® UHMWPE yarns, the shift is not based on the same stress for the different temperatures but the

same stress level at each temperature. The law used for the time-stress superposition by Luo and al. is therefore slightly adjusted:

$$\log(a_\tau) = -\frac{C1(\tau*\sigma_{break}(T)-\tau_0*\sigma_{break}(T))}{C3+(\tau*\sigma_{break}(T)+\tau_0*\sigma_{break}(T))} \quad (6)$$

With $C1$and $C3$, two variables depending on the material and the reference temperature, T the temperature, τ the percentage stress level, and τ_0 the reference percentage stress level, which is 40% of the stress at break at the temperature of each test. Results similar to Luo et al. [41] are found. Indeed, no matter the order of the superposition (time-temperature then time-stress level or time-stress level then time-temperature) the same final master curve is determined, the factors being multiplied. Sub master-curves achieved by time-stress level superposition are presented at each test creep temperature in Figure 17a, b, and c. Moreover, shift factors are more dependent on the stress level difference with the temperature, which is noticeable in Figure 17d, as underlined for the PMMA by Luo et al. [41]. Thanks to this TTSSP overlay, the creep behavior of the studied yarns could be reconstructed over a longer period (Figure 16e).

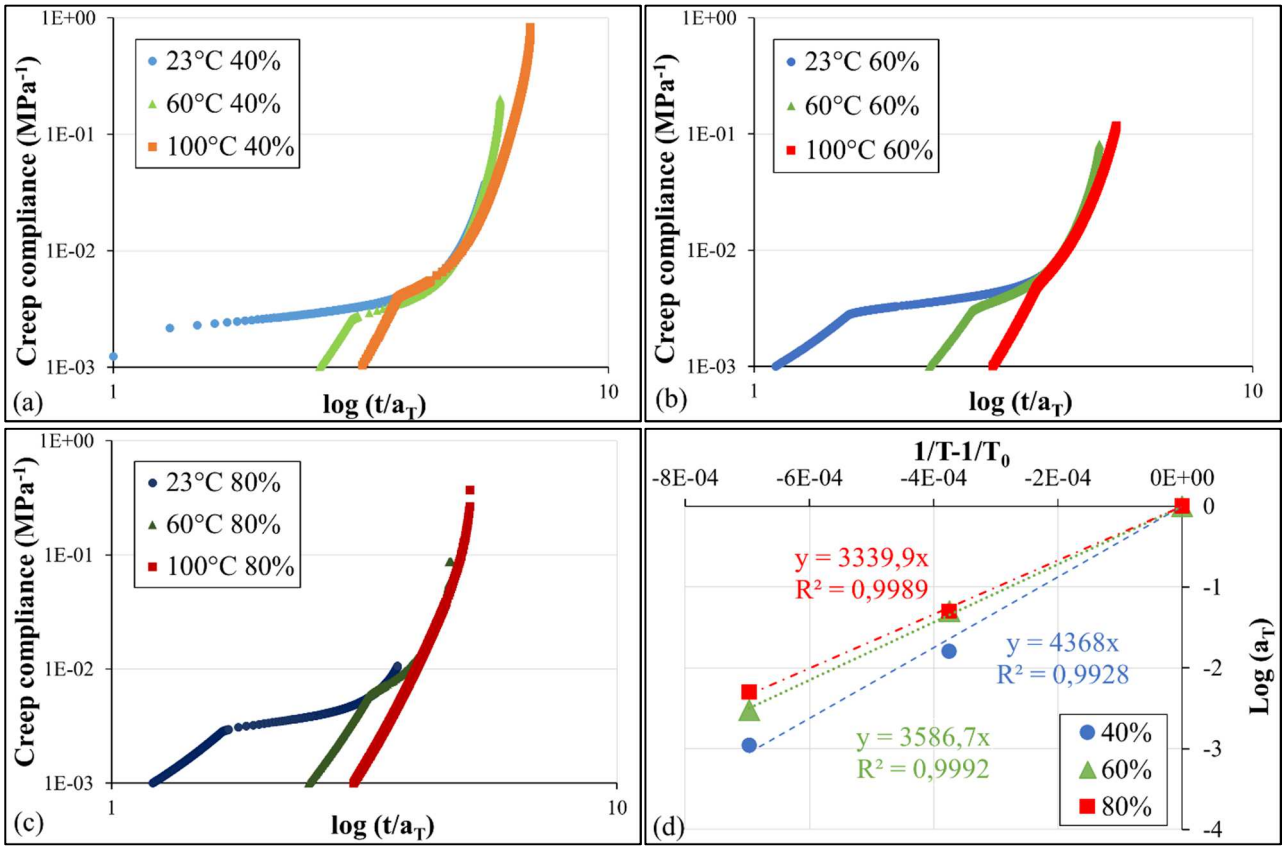

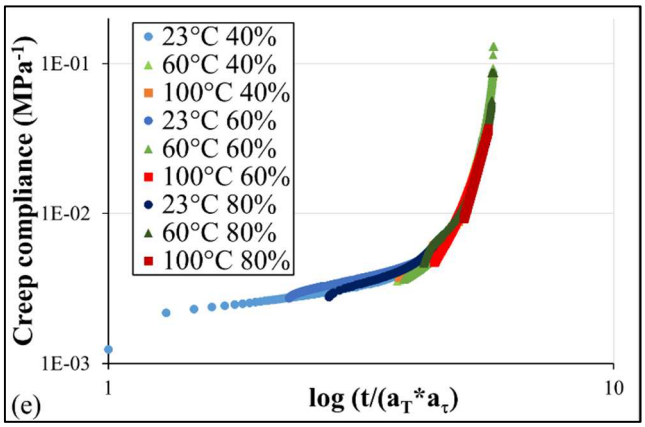

Figure 16. Master curves obtained by time-temperature superposition for (a) 40%, (b) 60% and (c) 80% of maximum load at each temperature; (d) Representative curves of the dependence of the shift factor on temperature; (e) Final master curve after time and stress level-superposition

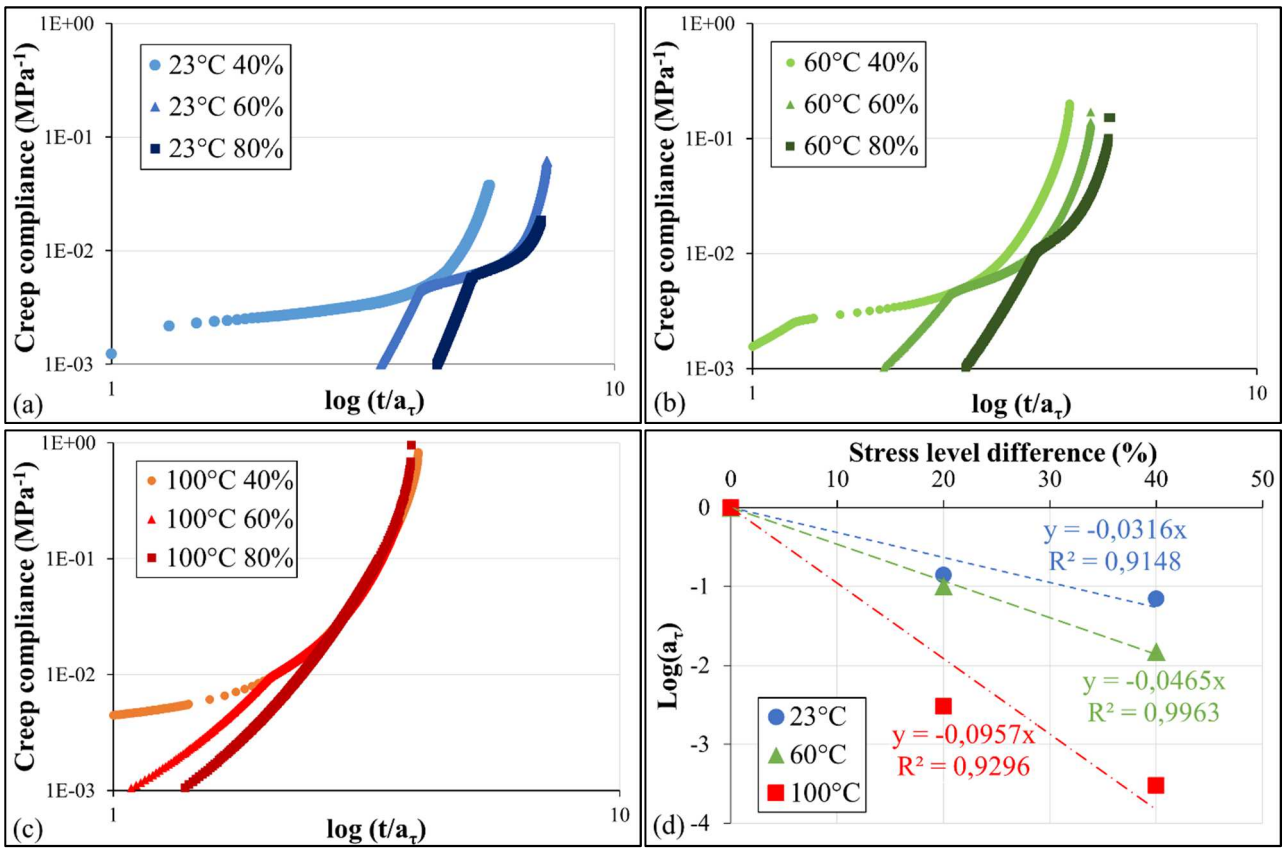

Figure 17. Master curves obtained by time-stress level superposition for (a) 23°C, (b) 60°C, and (c) 100°C; (d) Representative curves of the dependence of the shift factors on stress level difference in %

5 CONCLUSION

Doyentrontex® yarns have been fully characterized in tension, with monotonous and load-unload tests, at several temperatures and strain rates, as well as creep at several temperatures and load levels. First of all, before any thermomechanical characterization, a protocol was established by proposing the setup of the yarns, the crossbar speed as well as the useful length and the section to be considered. Temperature has a strong impact on the mechanical response of the yarns. Indeed, the rigidity and maximum strength decrease with temperature while the strain at break increases. The

same trends are found at high strain rates and low temperatures or low speeds and high temperatures. These different parameters can then be superposed and give a master curve, according to a WLF law or also an Arrhenius law modified for semi-crystalline polymers, to obtain their values at 23°C at the different strain rates. A transition occurs at very low strain rates (10^{-8} s^{-1} at 23°C or 10^{-4} s^{-1} at 100°C). A different behavior at 100°C from the other temperatures tested was also observed in load-unload and creep. Thus, given the hysteresis, the behavior at 100°C is of an elasto-viscoplastic type while at lower temperatures it is of a hyperelastic one, combined with plasticity. The behavior of these yarns is thereby very complex. It would be then necessary to relate these findings to the physical state of the yarns because behavior is highly dependent on morphology, and therefore, on the phases and chain conformations. Under certain stress and temperature conditions, phase transitions were observed. These results are therefore consistent with the literature. Regarding creep tests, the size of the three usual creep zones depends on the temperature. From these tests, a time-temperature-stress level superposition leads to the reconstruction of the yarns creep behavior over a long period at the reference temperature 23°C and the reference stress level which is 40% of the nominal stress at break in tensile tests at 23°C.

6 CREDIT AUTHOR STATEMENT

Coline Roiron: Methodology, Validation, Investigation, Writing-original Draft, Writing-Review & Editing, Visualization. **Eric Lainé:** Conceptualization, Writing-Review & Editing, Supervision. **Jean-Claude Grandidier:** Conceptualization, Writing-Review & Editing, Supervision. **Dominique Olivier:** Resources. **Nicolas Garois:** Conceptualization, Project administration, Supervision. **Cathie Vix:** Project administration.

7 AKNOWLEDGMENTS

The authors would like to thank the R&D Corporate department of Total Group for their financial support for this research.

8 REFERENCES

[1] E. Witten, V. Mathes, M. Sauer, et M. Kühnel, Composites Market Report 2018, Market developments, trends, outlooks and challenges, 2018.

[2] N. J. Capiati et R. S. Porter, The concept of one polymer composites modelled with high density polyethylene, *J. Mater. Sci.*, vol. 10, 1975, doi: 10.1007/BF00554928.

[3] C. Gao *et al.*, Preparation and characterization of uniaxial poly(lactic acid)-based self-reinforced composites, *Compos. Sci. Technol.*, vol. 117, 2015, doi: 10.1016/j.compscitech.2015.07.006.

[4] P. J. Hine, I. M. Ward, N. D. Jordan, R. Olley, et D. C. Bassett, The hot compaction behaviour of woven oriented polypropylene fibres and tapes. I. Mechanical properties, *Polymer*, vol. 44, n° 4, 2003, doi: 10.1016/S0032-3861(02)00809-1.

[5] P. Vecchione, D. Acierno, M. Abbate, et P. Russo, Hot-compacted self reinforced polyamide 6 composite laminates, *Compos. Part B Eng.*, vol. 110, 2017, doi: 10.1016/j.compositesb.2016.11.007.

[6] C. Schneider, S. Kazemahvazi, M. Åkermo, et D. Zenkert, Compression and tensile properties of self-reinforced poly(ethylene terephthalate)-composites, *Polym. Test.*, vol. 32, n° 2, 2013, doi: 10.1016/j.polymertesting.2012.11.002.

[7] P. Rojanapitayakorn, P. T. Mather, A. J. Goldberg, et R. A. Weiss, Optically transparent self-reinforced poly(ethylene terephthalate) composites: molecular orientation and mechanical properties, *Polymer*, vol. 46, n° 3, 2005, doi: 10.1016/j.polymer.2004.11.032.
[8] C. Marais et P. Feillard, Manufacturing and mechanical characterization of unidirectional polyethylene-fibre/polyethylene-matrix composites, *Compos. Sci. Technol.*, vol. 45, n° 3, 1992, doi: 10.1016/0266-3538(92)90086-I.
[9] M. Deng et S. W. Shalaby, Properties of self-reinforced ultra-high-molecular-weight polyethylene composites, *Biomaterials*, vol. 18, n° 9, 1997, doi: 10.1016/S0142-9612(96)00194-9.
[10] C. M. Wu, P. C. Lin, et R. Murakami, Long-term creep behavior of self-reinforced PET composites, *Express Polym. Lett.*, vol. 11, n° 10, 2017, doi: 10.3144/expresspolymlett.2017.78.
[11] N. Cabrera, B. Alcock, J. Loos, et T. Peijs, Processing of all-polypropylene composites for ultimate recyclability, *Proc. MECH E Part J. Mater. Appl.*, vol. 218, n° 2, 2004, doi: 10.1243/146442004323085563.
[12] I. M. Ward et P. J. Hine, The science and technology of hot compaction, *Polymer*, vol. 45, n° 5, 2004, doi: 10.1016/j.polymer.2003.11.050.
[13] A. L. dos Santos Alves, L. F. Cassiano Nascimento, et J. C. M. Suarez, « Influence of weathering and gamma irradiation on the mechanical and ballistic behavior of UHMWPE composite armor », *Polym. Test.*, vol. 24, n° 1, 2005, doi: 10.1016/j.polymertesting.2004.06.003.
[14] B. P. Russell, K. Karthikeyan, V. S. Deshpande, et N. A. Fleck, The high strain rate response of Ultra High Molecular-weight Polyethylene: From fibre to laminate, *Int. J. Impact Eng.*, vol. 60, 2013, doi: 10.1016/j.ijimpeng.2013.03.010.
[15] A. L. Forster *et al.*, Long-term stability of UHMWPE fibers, *Polym. Degrad. Stab.*, vol. 114, 2015, doi: 10.1016/j.polymdegradstab.2015.01.028.
[16] D. J. Dijkstra et A. J. Pennings, Annealing of gel-spun hot-drawn ultra-high molecular weight polyethylene fibres, *Polym. Bull.*, vol. 19, n° 5, 1988, doi: 10.1007/BF00263918.
[17] J. Smook, W. Hamersma, et A. J. Pennings, The fracture process of ultra-high strength polyethylene fibres, *J. Mater. Sci.*, vol. 19, n° 4, 1984, doi: 10.1007/BF01120049.
[18] R. S. Porter et L.-H. Wang, Uniaxial Extension and Order Development in Flexible Chain Polymers, *J. Macromol. Sci. Part C Polym. Rev.*, vol. 35, n° 1, 1995, doi: 10.1080/15321799508014590.
[19] L. Berger, H. . Kausch, et C. J. . Plummer, Structure and deformation mechanisms in UHMWPE-fibres, *Polymer*, vol. 44, n° 19, 2003, doi: 10.1016/S0032-3861(03)00536-6.
[20] F. X. Kromm, T. Lorriot, B. Coutand, R. Harry, et J. M. Quenisset, Tensile and creep properties of ultra high molecular weight PE fibres, *Polym. Test.*, vol. 22, n° 4, 2003, doi: 10.1016/S0142-9418(02)00127-7.
[21] B. Dessain, O. Moulaert, R. Keunings, et A. R. Bunsell, Solid phase change controlling the tensile and creep behaviour of gel-spun high-modulus polyethylene fibres, *J. Mater. Sci.*, vol. 27, n° 16, 1992, doi: 10.1007/BF00541588.
[22] M. . Wilding et I. . Ward, Tensile creep and recovery in ultra-high modulus linear polyethylenes, *Polymer*, vol. 19, n° 8, 1978, doi: 10.1016/0032-3861(78)90208-2.
[23] P. Schwartz, A. Netravali, et S. Sembach, Effects of Strain Rate and Gauge Length on the Failure of Ultra-High Strength Polyethylene Fibers, *Text. Res. J.*, vol. 56, n° 8, 1986, doi: 10.1177/004051758605600807.
[24] D. J. Dijkstra, J. C. M. Torfs, et A. J. Pennings, Temperature-dependent fracture mechanisms in ultra-high strength polyethylene fibers, *Colloid Polym. Sci.*, vol. 267, n° 10, 1989, doi: 10.1007/BF01410334.
[25] K. K. Phani, Evaluation of single-fibre strength distribution from fibre bundle strength, *J. Mater. Sci.*, vol. 23, n° 3, 1988, doi: 10.1007/BF01153993.

[26] Z. Chi, T.-W. Chou, et G. Shen, Determination of single fibre strength distribution from fibre bundle testings, *J. Mater. Sci.*, vol. 19, nº 10, 1984, doi: 10.1007/BF00549820.
[27] T. Peijs, E. A. M. Smets, et L. E. Govaert, Strain rate and temperature effects on energy absorption of polyethylene fibres and composites, *Appl. Compos. Mater.*, vol. 1, nº 1, 1994, doi: 10.1007/BF00567210.
[28] M. Matsuo et C. Sawatari, Temperature dependence of the crystal lattice modulus and the Young's modulus of polyethylene, *Macromolecules*, vol. 21, nº 6, 1988, doi: 10.1021/ma00184a022.
[29] L. E. Govaert et T. Peijs, Tensile strength and work of fracture of oriented polyethylene fibre, *Polymer*, vol. 36, nº 23, 1995, doi: 10.1016/0032-3861(95)96848-3.
[30] H. Van Der Werff et A. J. Pennings, Tensile deformation of high strength and high modulus polyethylene fibers, *Colloid Polym. Sci.*, vol. 269, nº 8, 1991, doi: 10.1007/BF00657441.
[31] M. A. Wilding et I. M. Ward, Creep and recovery of ultra high modulus polyethylene, *Polymer*, vol. 22, nº 7, 1981, doi: 10.1016/0032-3861(81)90259-7.
[32] M. A. Wilding et I. M. Ward, Creep and stress-relaxation in ultra-high modulus linear polyethylene, *J. Mater. Sci.*, vol. 19, nº 2, 1984, doi: 10.1007/BF02403251.
[33] L. E. Govaert et P. J. Lemstra, Deformation behavior of oriented UHMW-PE fibers, *Colloid Polym. Sci.*, vol. 270, nº 5, 1992, doi: 10.1007/BF00665989.
[34] P. J. R. Leblans, C. W. M. Bastiaansen, et L. E. Govaert, Viscoelastic properties of UHMW-PE fibers in simple elongation, *J. Polym. Sci. Part B Polym. Phys.*, vol. 27, nº 5, 1989, doi: 10.1002/polb.1989.090270504.
[35] L. E. Govaert, E. L. J. C. J. D'Hooghe, et A. A. J. M. Peijs, A micromechanical approach to the viscoelasticity of unidirectional hybrid composites, *Composites*, vol. 22, nº 2, 1991, doi: 10.1016/0010-4361(91)90669-8.
[36] L. Govaert, C. Bastiaansen, et P. Leblans, Stress-strain analysis of oriented polyethylene, *Polymer*, vol. 34, nº 3, 1993, doi: 10.1016/0032-3861(93)90546-M.
[37] Standard Test Method for Tensile Strength and Young's Modulus of Fibers C1557-03, 2004.
[38] M. R'Mili et M. Murat, Caractérisation des fibres par amélioration de l'essai sur mèche avec mesure directe de la déformation, *Comptes Rendus Académie Sci. - Ser. IIB - Mech.-Phys.-Chem.-Astron.*, vol. 324, nº 6, 1997, doi: 10.1016/S1251-8069(99)80046-3.
[39] P. B. McDaniel, J. M. Deitzel, et J. W. Gillespie, Structural hierarchy and surface morphology of highly drawn ultra high molecular weight polyethylene fibers studied by atomic force microscopy and wide angle X-ray diffraction, *Polymer*, vol. 69, 2015, doi: 10.1016/j.polymer.2015.05.010.
[40] J. T. Seitz et C. F. Balazs, Application of time-temperature superposition principle to long term engineering properties of plastic materials, *Polym. Eng. Sci.*, vol. 8, nº 2, 1968, doi: 10.1002/pen.760080211.
[41] W. Luo, C. Wang, X. Hu, et T. Yang, Long-term creep assessment of viscoelastic polymer by time-temperature-stress superposition, *Acta Mech. Solida Sin.*, vol. 25, nº 6, 2012, doi: 10.1016/S0894-9166(12)60052-4.